THE ANNALS OF "DUNAREA DE JOS" UNIVERSITY OF GALATI
FASCICLE XI – SHIPBUILDING. ISSN 1221-4620, e-ISSN 2668-3156
DOI: https://doi.org/10.35219/AnnUgalShipBuilding/2025.48.11
2025

ANALYSIS OF GLOBAL AND LOCAL STRENGTH USING 3D FEM MODELS OF THREE CARGO HOLDS IN A 47600 DWT CHEMICAL TANKER

Ștefan - Iulian Rață
"Dunarea de Jos" University of Galati, 47 Faculty of Naval Architecture, Galati, Domneasca Street, 800008, Romania,
E-mail: rata.iulian1999@gmail.com

Anișoara - Gabriela Cristea
"Dunarea de Jos" University of Galati, 47 Faculty of Naval Architecture, Galati, Domneasca Street, 800008, Romania,
E-mail: anisoara.cristea@ugal.ro

ABSTRACT

This study examines both the global and local structural strength of a 3D finite element model (FEM) representing the three cargo holds of a 47600-DWT chemical tanker. Vessels of this type require a detailed assessment of their structural behavior under extreme loading conditions as well as routine operational demands. The analysis of stress distribution and structural strength enables the identification of critical areas within the hull, providing essential insights for enhancing the vessel's structural integrity and overall performance.

Keywords: chemical tanker, finite element method, stress concentration, structural strength analysis, global and local strength, hull girder structure, ship structural integrity.

1. INTRODUCTION

The vessel examined in this study is a 47600 DWT chemical tanker designed to transport chemical products and petroleum derivatives. Its primary role is to ensure the safe and efficient carriage of bulk chemicals in accordance with strict international standards and regulations. Given the sensitive and potentially hazardous nature of its cargo, preserving the ship's structural integrity is essential for preventing accidents and safeguarding marine environment.

This study analyzes the global and local strength of a 3D finite element model (FEM) spanning three cargo holds and assesses the resulting implications for the vessel's structural robustness and durability during operation.

The vessel's principal dimensions were sourced from the Shipbuilding and Marine Engineering in Japan 2007 database, which provides key specifications for ships constructed in that year. These data are summarized in **Table 1.1**.

Using this information, the vessel's structural modeling was performed with the Poseidon ND v.21.4 software, developed by the DNV classification society.

Table 1.1 Dimensional characteristics of the simplified model

Dimensional characteristics	Value	Unit

Dimensional characteristics	Value	Unit
Lbp - length between perpendiculars	172	[m]
LOA - overall length	182.84	[m]
B - beam	32.2	[m]
D - depth of construction	17.1	[m]

2. DEVELOPMENT AND ANALYSIS OF THE SIMPLIFIED MODEL

The transverse section of the midship area, obtained using the Poseidon software, served as the basis for modeling the central part of the vessel, where the structural loads are most representative for finite element analysis. Consequently, the 3D geometry was developed over a span of three cargo holds, considering symmetry and modeling only one half of the ship's hull.

The model construction process was performed in sequential stages: defining the characteristic points of the transverse section, generating the principal structural curves (keel, girders, and longitudinal stiffeners), and subsequently creating the enclosing surfaces.

These geometric entities were then used to generate the 3D component surfaces, as shown in the following figures, forming the basis for the subsequent finite element mesh discretization.

2.1 3D CAD modeling using FEMAP/NX Nastran

Using FEMAP/NX Nastran, the 3D-CAD model of the midship structure (**Fig. 2**) provides a detailed framework for assessing the vessel's structural performance. This digital representation allows engineers to configure and evaluate structural components while ensuring full compliance with international safety and efficiency standards. The analyses performed on this model are instrumental in identifying potential failure regions, improving overall structural integrity, and reducing environmental risks arising from structural damage or cargo leakage.

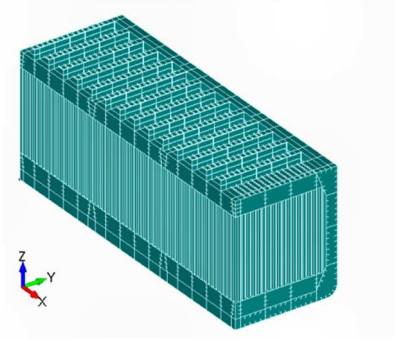

Fig. 2 "3D CAD" - model for finite element analysis (FEA)

3. MATERIAL PROPERTIES AND MESHING PROCEDURE

The analyzed midship structure consists of marine-grade high-strength steel, whose mechanical properties are summarized in **Table 1.2**. To obtain an accurate and computationally efficient 3D finite element (FEM) model, the 3D-CAD geometry was discretized using plate-type finite elements in two configurations: a quadrilateral-element mesh and a triangular-element mesh. Each topology was generated at three refinement levels—fine (100 mm), medium (150 mm), and coarse (200 mm)—based on the element edge length.

Table 1.2 Material mechanical characteristics

Description	Value	Unit
Yield strength (σ_c)	235	MPa
Longitudinal elastic modulus (Young's modulus - E)	210	GPa
Poisson's ratio (ν)	0.3	-
Density (ρ)	7800	kg/m^3

This modeling strategy enables a systematic evaluation of the influence of both element topology and mesh refinement on the global structural behavior of the model. Separate meshes were created for each con-

figuration and subsequently employed in static analyses to compare the effects of mesh density and computational efficiency. Using this approach, the effectiveness of steel plate beveling and its influence on the vessel's structural performance can be systematically evaluated (**Table 1.3**).

Table 1.3 Features of the 3D finite element model (3D-FEM)

Element type	Element size [mm]	Number of nodes	Number of elements
Quad	100	1241739	1269289
	150	590284	609265
	200	358393	373849
Tri	100	1277005	2607961
	150	582947	1202755
	200	350520	731018

The characteristics of the 3D FEM models (**Figures 4 and 5**) emphasize the influence of mesh discretization on the overall complexity and accuracy of the structural analysis. Selecting an appropriate mesh size is critical to maintaining an effective balance between computational efficiency and analytical precision within the simulations.

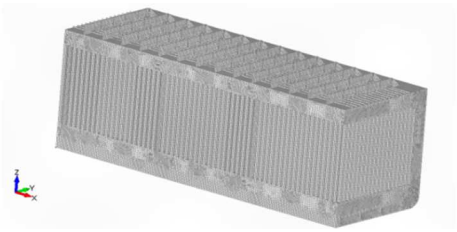

Fig. 4 Complete 3D - FEM model (quad)

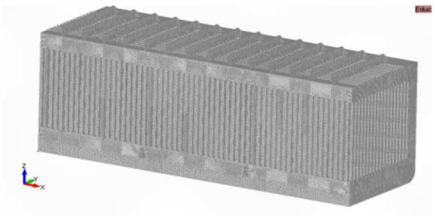

Fig. 5 Complete 3D - FEM model (tri)

4. BOUNDARY CONDITIONS

To simulate the vessel's geometric symmetry, boundary constraints were applied along the longitudinal corrugated bulkhead located in the centerline plane (**Table 1.4** and **Fig. 6**). This modeling strategy allows for an accurate representation of the symmetry boundary conditions while significantly reducing the computational demand of the finite element analysis.

To maintain consistent load transfer and effectively capture the interaction between finite elements, master nodes were introduced at both extremities of the model — the bow and the stern. These nodes were placed on the ship's centerline plane at a height of 7799 mm (**Figures 7**), corresponding to the neutral axis of the transverse section, which defines the reference for load application and global equilibrium constraints.

Table 1.4 Boundary conditions

Boundary condition	Blocked degrees of freedom					
	Ux	Uy	Uz	Rx	Ry	Rz
Symmetry in the diametral plane	-	*	-	*	-	-
Fore master nodes	-	*	*	*	-	*
Aft master nodes	*	*	*	*	-	*

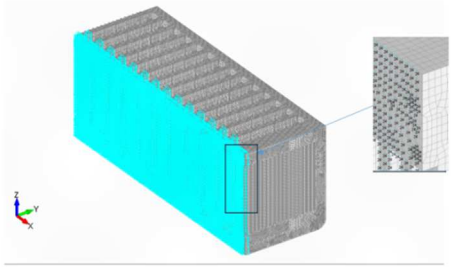

Fig. 6 Boundary condition setup for the diametral plane

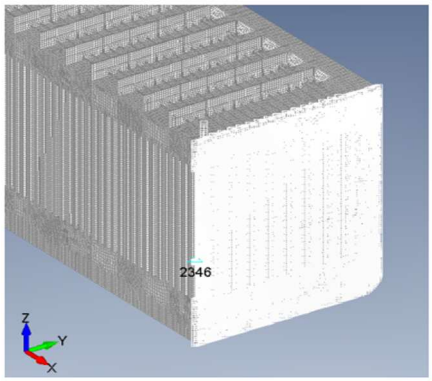

Fig. 7 Boundary conditions on the fore master nodes

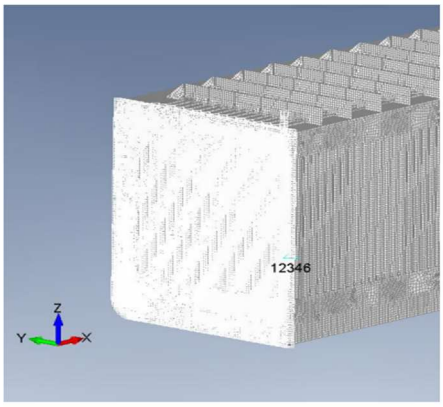

Fig. 8
Boundary conditions on the aft master nodes

5. LOADS APPLIED TO THE MODEL

A) Static loading condition in still water

To simulate realistic service conditions, the 3D finite element model was analyzed under the following load cases (**Fig. 9**):

✓ Gravitational load: represents the self-weight of the structural components and other onboard elements, calculated based on the steel density (ρ = 7.8 t/m³) and gravitational acceleration (g = 9.81 m/s²).

✓ b) Hydrostatic pressure of the cargo: Acting on the inner shell of the cargo hold, this pressure extends to a maximum height of H = 15280 mm, representing the highest tank filling level. The cargo, assumed to be oil, was considered to have a density of ρ = 0.9 t/m³.

✓ c) Hydrostatic pressure of seawater: generated by seawater (ρ = 1.025 t/m³) and applied to the external shell of the model up to a height of T = 12800 mm, corresponding to the ship's full-load draft.

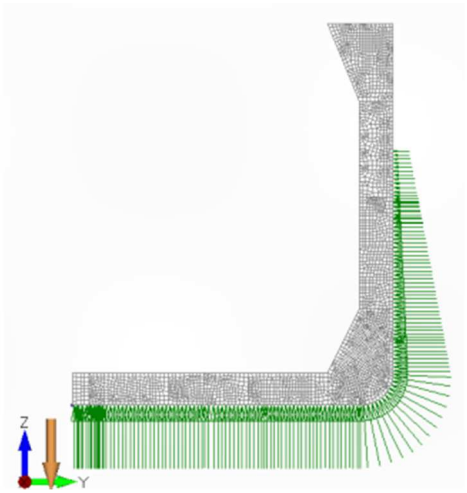

Fig. 9 Applied loads on the model for the static still-water loading condition

B) Static loading condition on waves

The same model was further analyzed under wave conditions to evaluate the vessel's structural response. The following load cases were applied (**Table 1.5**, **Figures 10** and **11**):

✓ a) Gravitational loading: identical to the one applied in the static still-water case described previously.

✓ b) Hydrostatic pressure of the cargo: the same as in the preceding stillwater scenario**.**

c) Quasi-Static equivalent wave loading: expressed as an equivalent hydrostatic pressure (in N/mm²) and determined from the balancing parameters shown in **Table 1.5.** (**Figures 10** and **11**).

Table 1.5 Balancing parameters derived from the simplified 1D analysis

Description - parameters	Value	U.M.
LOA - length of the ship	182840	mm
HW - Wave height	6951	mm
XPP - Aft end of the model	67420	mm
DPP - aft draft	12800	mm
DPV - forward draft	12800	mm

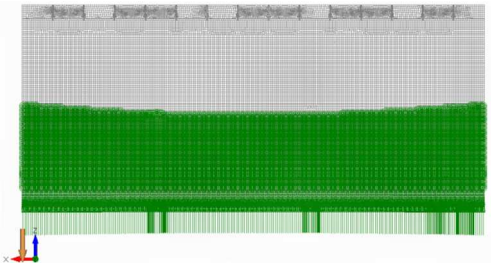

Fig. 10 Applied loads on the model for the case of static settling in a wave trough

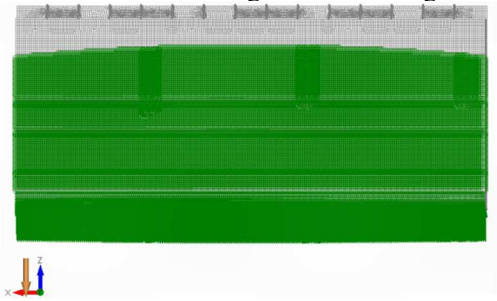

Fig. 11 Applied loads on the model for the case of static settling at the crest of a wave

6. "VON - MISES" STRESSES AND MAXIMUM DISPLACEMENTS IN THE SIMPLIFIED MODEL

A comparative summary of the Von-Mises stress values and maximum displacements for the simplified model, subjected to different load conditions and mesh configurations, is presented in the following table **(Table 1.7 and Table 1.8).**

The obtained data enable a comparasion of the effects of mesh type, element size, and loading condition on the structural behavior.

This approach provides valuable insights into the accuracy and stability of the finite element model, allowing for the identification of the optimal mesh configuration that ensures both computational efficiency and reliable stress and displacement predictions.

Table 1.7 Von-Mises stresses and maximum displacements of the simplified model using quadrilateral elements

Quadrilateral elements

Ship positioning case		Mesh discretization			UM.
Von - Mises Stress	Still water	200	150	100	[mm]
		140.24	146.2	148.78	[MPa]
	Sagging	200	150	100	[mm]
		252.39	272.7	295.94	[MPa]
	Hogging	200	150	100	[mm]
		273.27	283.66	317.74	[MPa]
Displacements	Still water	200	150	100	[mm]
		6.28	6.4	6.51	[mm]
	Sagging	200	150	100	[mm]
		25.49	25.43	25.56	[mm]
	Hogging	200	150	100	[mm]
		28.49	28.38	28.61	[mm]

Table 1.8 Von-Mises stresses and maximum displacements of the simplified model using triangular elements

Triangular elements

Ship positioning case		Mesh discretization			UM.
Von - Mises Stress	Still water	200	150	100	[mm]
		131	138.69	141.16	[MPa]
	Sagging	200	150	100	[mm]
		358.83	343.57	435.67	[MPa]
	Hogging	200	150	100	[mm]
		329.58	317.84	368.86	[MPa]
Displacements	Still water	200	150	100	[mm]
		5.85	6.66	6.24	[mm]
	Sagging	200	150	100	[mm]
		25.04	22.6	25.36	[mm]
	Hogging	200	150	100	[mm]
		27.9	30.36	28.43	[mm]

7. INTERPRETATION OF RESULTS

a) Still water condition

Although the differences between the results are relatively small (**Fig 11**), they become more noticeable when using quadrilateral elements. This behavior may suggest a more accurate representation of the structural reality or a positive influence of mesh resolution on the precision of the results.

The quadrilateral mesh is preferable when higher accuracy is desired, particularly in regions characterized by linear structural behavior and regular geometry. Conversely, the triangular mesh proves useful in areas with complex geometries or when rapid and automatic meshing required, although it introduces an additional degree of stiffness.

For the analyzed case, the differences between the two element types are minor, indicating a good quality of discretization for both configurations. As the average finite element size decreases, both quadrilateral and triangular meshes yield more accurate results, converging toward a stable solution. This behavior demonstrates that a refined model captures stress distribution and local deformation states more accurately.

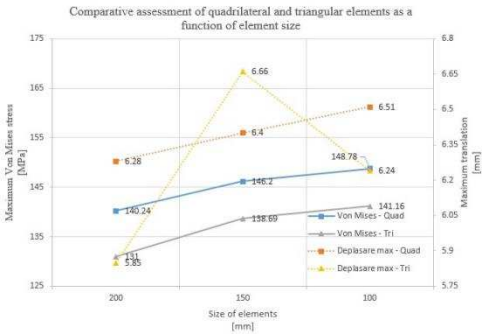

Fig. 11 Comparative assessment of quadrilateral and triangular elements as a function of element size for the still-water condition

b) Sagging condition

The Von-Mises stresses obtained represent key indicators of the maximum stress at a given point within the structure and were used to verify whether the material remains within allowable limits under the applied loads. The results show that, as the element size decreases, the stress values increase - consistent with the principles of finite element analysis.

Comparing the two element types (**Fig. 12**), triangular elements generate significantly higher Von-Mises stress values than quadrilateral elements, particularly for the finer mesh (435.69 MPa versus 295.97 MPa). This discrepancy is attributable to the triangular elements' ability to more accurately capture local stress variations, alongside their known tendency to overpredict stresses in regions with steep gradients.

The analyses performed for the ship positioned in a wave trough indicate that the maximum total deflection remains within an approximately constant range (25–25.5 mm), suggesting good solution convergence and minimal influence of element type and size on global deflection. An exception was observed for the 150 mm triangular mesh,

where the maximum deflection decreased to 22.6 mm, potentially indicating a local discretization anomaly or numerical stiffening that could affect local accuracy.

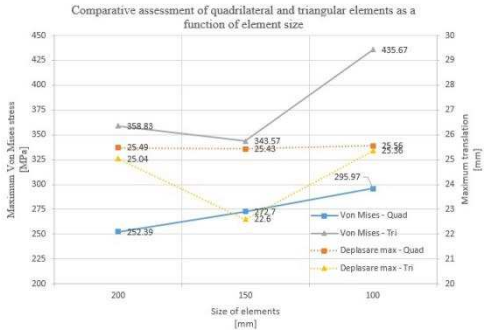

Fig. 12 Comparative assessment of quadrilateral and triangular elements as a function of element size for the sagging condition

c) Hogging condition

A progressive increase in maximum stresses was observed with mesh refinement, which is characteristic of finite element analyses. The triangular element formulation consistently yielded higher Von-Mises stress values compared to quadrilateral elements, particularly at the 100 mm size (**Fig. 13**). This outcome suggests heightened sensitivity to localized stress variations or strain concentration within transitional regions, an expected consequence of the triangular element stress distribution characteristics.

Maximum deflections obtained with the quadrilateral mesh demonstrated remarkable stability, with only marginal variations, indicating robust numerical behavior and adequate discretization. Conversely, triangular elements exhibited greater variability, ranging from 27.9 mm to 30.36 mm. This disparity may indicate localized element distortion, sensitivity to nodal placement, or the need for further mesh refinement.

This comparative behavior justifies the preferential use of quadrilateral elements in critical structural areas where solution precision and stability are essential. For zones of high stress concentration, reduced-size quadrilateral elements (100 mm) are recommended for a faithful representation of stress distribution. For preliminary analysis or rapid estimation, 150 mm quadrilateral elements provide an effective compromise between result accuracy and computational cost.

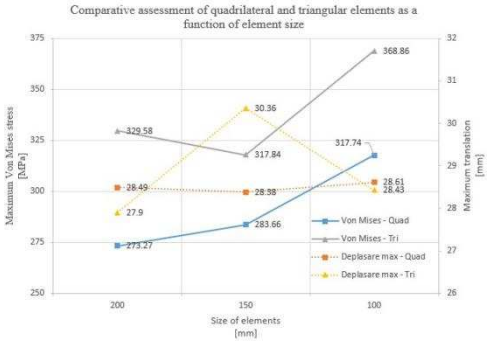

Fig. 13 Comparative assessment of quadrilateral and triangular elements as a function of element size for the hogging condition

8. CONCLUSIONS

The analysis, performed on an extended 3D FEM model spanning the length of three cargo holds and subjected to three hydrostatic loading scenarios (still water, wave trough, and wave crest), aimed to evaluate the structural behavior as a function of the type and degree of refinement of the finite element mesh. The model was discretized using both triangular and quadrilateral finite elements, each at three element sizes (200 mm, 150 mm, and 100 mm), to assess their influence on the distribution of Von-Mises stresses and maximum deflection.

The results consistently indicated the emergence of peak stresses at the junction between the upper longitudinal and transverse stiffeners, particularly in the vicinity of the centerline, where the structure experiences the highest constraints. These stress concentrations are attributed to localized, numerically induced stiffening. The highest Von-Mises stress recorded was 435.67 MPa

for the 100 mm triangular elements under the wave trough condition, whereas the maximum value obtained for quadrilateral elements was 317.74 MPa, recorded during the wave crest condition.

Mesh refinement had a direct impact on the analysis precision: smaller element sizes led to a more realistic estimation of stress gradients but significantly increased computation time. In general, quadrilateral elements offered superior numerical stability and greater consistency of results. Conversely, triangular elements, while advantageous in areas with complex geometry, tended to locally overpredict stresses and required more careful refinement.

Maximum deflections exhibited minimal variation with quadrilateral elements, indicating good solution convergence, while significant variations were observed with triangular elements.

It is important to emphasize that the model analyzed was idealized, omitting actual stiffening components such as brackets or internal stiffeners. In practical applications, these elements contribute substantially to the reduction of local stresses, particularly in critical regions such as stiffener junctions or technological cutouts. Consequently, the stress values obtained in this analysis should be interpreted as conservative estimates.

Acknowledgment

The author wishes to express their profound gratitude to the Department of Naval Architecture and the Research Center of the Faculty of Naval Architecture at "Dunarea de Jos" University of Galati for the invaluable institutional support provided throughout the duration of this research project. Their contribution was instrumental in the successful completion of the numerical analyses and the thorough evaluation of the structural model.

We specifically acknowledge the provision of essential resources and infrastructure necessary for conducting the extended 3D FEM simulations presented herein. Furthermore, the authors are deeply thankful for the continuous academic guidance, expert technical advice, and enduring encouragement received from the faculty members, which were indispensable at every stage of the study—from the initial conceptualization to the final presentation of the results.

REFERENCES

[1] Cristea A.G., *Contribuții privind optimizarea structurilor de navă*, Teză de doctorat, Galați, 2014

[2] Alexandru George Gheorghe, Anișoara-Gabriela Cristea, *Analysis of the impact of local discretization in the area of technological cutouts on stress concentrators, The a*nnals of" Dunarea de Jos" University of Galati. Fascicle XI Shipbuilding, 2024

[3] Nicușor-Dănuț Ilie, Anișoara - Gabriela Cristea, A*nalysis of stress and deformations in the transverse walls of a 50100 tdw tanker*, The annals of "Dunarea de Jos" University of Galati Fascicle XI Shipbuilding, 2023

[4] **DNV,** *"Rules for Classification. Maritime Ships"*, Det Norske Veritas, Novik, 2025.

[5] **FEMAP**, "*Femap/NX Nastran User Guide. Academic License*", Siemens PLM Software, 2025.

[6] Lee, S.C.; Doh, D.H.; Goo, J.S. *Analysis of wave loads of ships with advancing speed in regular waves.* J. Korea Soc. Power Syst.Eng. 2010,

[7] **Reddy, J.N**, "*An Introduction to the Finite Element Method. Third Edition"*, McGraw Hill Publishing House, New York, 2006.

[8] http://www.iacs.org.uk/publications/common-structural-rules/csr-for-bulk-carriers-and-oil-tankers/

Paper received on October 28th, 2025